Click Here for Full Article

Ion composition and pressure changes in storm time and nonstorm substorms in the vicinity of the near-Earth neutral line

L. M. Kistler,[1] C. G. Mouikis,[1] X. Cao,[1] H. Frey,[2] B. Klecker,[3] I. Dandouras,[4] A. Korth,[5] M. F. Marcucci,[6] R. Lundin,[7] M. McCarthy,[8] R. Friedel,[9] and E. Lucek[10]

[1] Using CLUSTER/CODIF data from close to ∼19 Re in the magnetotail, we have performed a superposed epoch analysis of storm time and nonstorm substorms to determine how the ion composition changes during a substorm. We find that the median O^+ density and pressure in the plasma sheet are a factor of 5 higher during storm times than during nonstorm times. However, we do not observe significant changes in the composition during a substorm that would indicate that ionospheric outflow is playing a dynamic role in loading the plasma sheet or triggering the substorm at this location. There are differences between the storm time and nonstorm substorms, and it is intriguing to consider whether the composition differences play a role. The storm time substorms exhibit more loading and faster unloading than the nonstorm substorms. In addition, we observe differences in the H^+ and O^+ behavior at onset in the storm time substorms that we attribute to the different dynamics of the two ion species at the reconnection site and during the field reconfiguration due to their different gyroradii. The H^+ density and pressure decrease over the whole energy range at substorm onset, while the O^+ density and pressure decrease less, and the O^+ temperature increases. That more O^+ is left after substorm onset indicates that either the O^+ is more quickly replenished from O^+ in the lobes and/or that the more energetic O^+, due to its larger gyroradius, is not depleted when the field reconfigures and is accelerated in the thin current sheet.

Citation: Kistler, L. M., et al. (2006), Ion composition and pressure changes in storm time and nonstorm substorms in the vicinity of the near-Earth neutral line, *J. Geophys. Res.*, *111*, A11222, doi:10.1029/2006JA011939.

1. Introduction

[2] The purpose of this paper is to determine the differences between H^+ and O^+ behavior in storm time and nonstorm substorms and, from these observations, to determine if additional O^+ in the plasma sheet has an impact on substorm behavior. It is well known that the O^+ content of the ring current increases during storms. Since the ring current is formed by increased convection from the nightside plasma sheet, it would be expected that the plasma sheet also contains significant O^+ during these

times. However, it has not been established whether the plasma sheet during active substorm times always has significant O^+ or whether it is only present during storm times. The O^+ content of the plasma sheet is known to increase with activity [*Lennartsson and Shelley*, 1986], but no study has specifically shown a difference between storm time and nonstorm time activity. Individual case studies [*Kistler et al.*, 2005; *Nose et al.*, 2005] have shown examples where O^+ is in fact the dominant ion species in the plasma sheet during storm time events. The source of O^+ in the magnetosphere is outflow from the ionosphere in the high-latitude regions, from both the dayside cusp and the nightside aurora [*Yau et al.*, 1984, 1985]. Both the cusp outflow and the nightside outflow increase with magnetospheric activity [*Yau et al.*, 1985; *Wilson et al.*, 2004; *Oieroset et al.*, 1999]. Modeling of single particle trajectories [*Winglee*, 2003] has shown that heavy ions from both the cusp and the nightside aurora have preferential access to the nightside near-Earth plasma sheet. *Sauvaud et al.* [2004] showed examples both of an injection of O^+ from the nightside aurora into the plasma sheet, and O^+ beams in the lobes, which presumably came from the cusp, confirming that both sources are observed in the near-Earth tail during active times. Thus we expect that when ion outflow is high, the near-Earth plasma sheet will be heavy-ion rich.

---

[1]Space Science Center, University of New Hampshire, Durham, New Hampshire, USA.

[2]Space Sciences Laboratory, University of California, Berkeley, California, USA.

[3]Max-Planck Institut für Extraterrestriche Physik, Garching, Germany.

[4]Centre d'Etude Spatiale des Rayonnements, Toulouse, France.

[5]Max-Planck Institut für Aeronomie, Katlenburg-Lindau, Germany.

[6]Istituto Fisica dello Spazio Interplanetario, Rome, Italy.

[7]Swedish Institute of Space Physics, Kiruna, Sweden.

[8]Geophysics Program, University of Washington, Seattle, Washington, USA.

[9]Space Science and Application, Los Alamos National Laboratory, Los Alamos, New Mexico, USA.

[10]Space and Atmospheric Physics, Blackett Laboratory, Imperial College London, London, UK.

[3] A high concentration of heavy ions in the plasma sheet may have an impact on the dynamics of the plasma sheet. The higher mass density would decrease the Alfven speed which would be expected to decrease the reconnection rate [*Shay and Swisdak*, 2004]. In addition, the higher mass density could decrease the threshold for the ion tearing mode instability, as suggested by *Baker et al.* [1982], making reconnection more likely to occur. This instability is triggered when the ions become unmagnetized in the thin plasma sheet. Because the growth rate is proportional to the ion gyroradius, a large heavier ion content increases the instability. *Baker et al.* [1985] looked for evidence of this in the CDAW 6 event. This event consisted of two substorms. The first one was localized in the 0200–0300 LT sector and occurred when the plasma sheet was predominantly composed of H^+ and He^{++}. This first substorm resulted in significant O^+ being added to the plasma sheet. The second substorm occurred much farther westward than the original substorm. They interpreted this as an example where the increased O^+ abundance in the plasma sheet may have effected the location of the substorm onset.

[4] *Daglis et al.* [1990] observed that in the near-Earth (8–9 Re) plasma sheet during a substorm, the largest increase in energy density was observed for O^+, and the O^+ energy density peaks just prior to the flux dropout. They suggest that O^+ contributes to the curvature current in this region, accelerating the tail stretching during the growth phase. In order to test whether O^+ does make the magnetotail more unstable, *Lennartsson et al.* [1993] performed a statistical study using the ISEE data set, looking explicitly for evidence that more or larger substorms were triggered when O^+ was enhanced, either due to geomagnetic activity, as measured by AE, or due to enhanced EUV. They found that the O^+ had no effect. *Daglis and Sarris* [1998] argued that the long time averages used in the Lennartson study would mask the effects of O^+, if they were from short-lived localized enhancements. Additionally, it is possible that the increase occurs at energies below the 100 eV lower limit of the ISEE instrument. At this point, more evidence is needed to substantiate the potential influence of O^+.

[5] If storm time substorms have more oxygen, it is possible that this impacts the development of the storm. The relationship between storms and substorms, and whether substorms that occur during storms are different from other substorms is controversial. *Baumjohann et al.* [1996] performed a superposed epoch analysis of plasma moments (without composition) and magnetic field data from 10 to 20 Re using AMPTE/IRM data and found that the dipolarization during storm time substorms occurred immediately after substorm onset, and the average magnetic elevation angle reached nearly 50 degrees, whereas the average dipolarization during nonstorm substorms is much more gradual and reaches a maximum elevation of only 15 degrees. In addition, they found that the temperature was higher during storm time substorms, both before and after onset. They conclude that the significant dipolarization during storms would bring the heated plasma close to Earth, contributing to the decrease in the *Dst*. *McPherron and Hsu* [2002] performed a similar study with a larger data set and found no significant differences between the time profile of the dipolarization and percent change of the total pressure between their storm time and nonstorm events. They also

found no significant differences between the changes in *Bz* in the lobe or the central plasma sheet between storm and nonstorm times. Thus they concluded that there was no qualitative difference between the substorm types. *Schoedel et al.* [2002] compared the average plasma moments in the plasma sheet during storm times and nonstorm times. They found enhanced rates of earthward flux transport during storm times in the 20–30 Re plasma sheet, and significantly reduced rates further in. They hypothesized that this may explain the need for the stronger dipolarizations observed by *Baumjohann et al.* [1996].

[6] The role of composition in storms and substorms is also controversial. *Fu et al.* [2002] showed that there was substantially more O^+ in storm time substorm injections than in nonstorm events. However, *Grande et al.* [2003], using CRRES data, found little change in *Dst* associated with substorms that occurred during a storm. In addition, using a superposed epoch analysis of dispersionless injections, they found that while the O^+/He^{++} density ratio was higher during storm times, indicating a greater ionospheric source, the change in composition during the substorm was about the same. Thus they conclude that the additional O^+ observed in storm time substorms does not make the substorms dynamically different. *Korth et al.* [2003], on the other hand, examining individual storm time and nonstorm time events in the CRRES data set, found that the O^+/H^+ energy density increase was significantly higher during storm time substorms than during nonstorm substorms. It is not clear why the different methods of analysis led to different results in the near-geosynchronous region.

[7] In this study we use CLUSTER data to investigate the differences between storm time and nonstorm time substorms in the plasma sheet at about 19 Re, which is in the vicinity of the near-Earth neutral line during a substorm. As this is the location where reconnection is taking place, the composition here should be the most important for determining whether the heavy ions are affecting the onset of reconnection or the reconnection rate. We have scanned individual events to determine whether the radial location of reconnection is statistically different during storm time and nonstorm time cases. We have then performed a superposed epoch analysis of the different substorm types to determine the statistical differences in the plasma composition and composition changes and whether there are obvious differences in the plasma dynamics.

2. Instrumentation and Data Selection

[8] The CLUSTER satellites are in polar orbits with an apogee of 19 Re and a perigee of 4 Re. The data used in this study are from the CODIF sensor of the CIS instrument [*Reme et al.*, 2001] and the magnetometer instrument (FGM) [*Balogh et al.*, 2001]. CODIF measures the three-dimensional distribution functions of the major ion species over the energy per charge range 40–40,000 eV/e. It is a combination of a top-cap electrostatic analyzer followed by postacceleration of 15 kV and then a time-of-flight measurement. It can resolve the major ion species, H^+, He^{++}, He^+, and O^+. For this paper we will concentrate on observations of H^+ and O^+ in the plasma sheet. The moments of the distribution used in this study are calculated over the energy range of 40–40,000 eV/e. This energy

range is expected to include the bulk of the density and pressure for most time periods, but there are cases where significant populations may fall outside this range. In the lobe regions there may be cold ions that contribute to the density, which would be missed by this instrument. In the plasma sheet, some fraction of the total pressure may be missed because of the 40 keV cutoff. *Kistler et al.* [1992], using an instrument on AMPTE/IRM with a higher maximum energy range, determined the peak contribution to the plasma pressure for H^+ before and after substorm onset for a number of events. Three of their events were for time periods when IRM was close to apogee at 18.8 Re, close to the CLUSTER apogee location. For these events, the energy range with the maximum contribution to the pressure after substorm onset was at $10-20$ keV and the contribution dropped off sharply above 30 keV. Before onset, the peak contribution was always from lower energies. Thus for H^+ we are confident that the majority of the pressure is being measured. The O^+ spectra are harder than the H^+ spectra after onset, so the peak contribution is at higher energies. Thus the O^+ pressure moment may be missing some of the pressure after substorm onset. In some storm time postonset time periods, the contribution to the pressure is still increasing at the highest CODIF energy channel. Thus after onset, the O^+ pressure is underestimated in some cases. The contribution to the density, however, is not significant above 40 keV.

[9] To identify substorm onsets, we first identified time periods when the CLUSTER satellites were located in the magnetotail, encountering the plasma sheet either intermittently or continuously, between 2030 and 330 MLT during the years $2001-2004$. For these time periods, we used both observations of dispersionless injections at geosynchronous orbit using LANL proton and electron data, and observations of auroral brightenings using the IMAGE FUV satellite to identify onsets. Independent lists of onsets from the two data sets were compiled. The $2001-2002$ onsets identified using IMAGE/FUV are given by *Frey et al.* [2004]. Altogether there were 451 substorm onsets identified during these times. Each onset was put into one of three categories: (1) onset time agrees within 10 min from the two data sources, (2) a clear onset is observed in one data set, while the other data set has no data, or (3) there is a clear onset in one data set, and no corresponding onset in the other. Events that fell into the first two categories were used for this study. Out of the 451 onsets, 138 were observed in both data sets, 195 were observed by LANL satellites when IMAGE had no data, and 11 were observed by IMAGE when the LANL satellites had no data, giving a total of 344 events satisfying categories 1 and 2. Forty events were observed by LANL, with no corresponding onset observed in IMAGE, and 67 events were observed in IMAGE with no corresponding event in the LANL data. These events were not used. The events were then categorized as main phase storm time, recovery phase storm time, or nonstorm time. A time period was considered a storm if the minimum *Dst* reached a value less than -50 nT. The main phase includes the time from the beginning of the storm, judging by either the start of a sudden storm commencement (SSC), or the start of the drop in *Dst*, to 2 hours after the minimum *Dst*. Recovery phase events include data from 2 hours after the minimum *Dst*, until the *Dst* returns to its prestorm value.

Finally, the main emphasis of the data analysis was on the behavior of the central plasma sheet. Thus for the superposed epoch analysis described in the next section, there had to be data from the central plasma sheet, defined as beta >1.0, during the 4 hour interval from 2 hours before to 2 hours after substorm onset. There were 33 main phase substorms, 32 recovery phase substorms, and 138 nonstorm substorms that satisfied all criteria and had CLUSTER/CODIF data in the central plasma sheet. Figure 1 shows the distribution of these events projected into the X-Y and X-Z planes. From top to bottom, Figure 1 shows the spacecraft location for the nonstorm, storm main phase, and storm recovery phase substorm onsets.

3. Data Analysis

3.1. Two Individual Substorm Events

[10] Figure 2 shows data from two substorms. On the left is shown data from a substorm on 11 October 2001, which occurred during a nonstorm period, and on the right is data from a substorm on 1 October 2001, which occurred during the main phase of a geomagnetic storm. The same two substorms were shown by *Kistler et al.* [2005]. Figure 2a gives the total pressure (magnetic plus plasma). Figure 2b gives the plasma beta. In both cases the satellites remained in the central plasma sheet, with beta around 1, throughout the time period. Figures 2c and 2d show the H^+ and O^+ differential flux, as a function of energy. Figure 2e shows the H^+ velocity in x. Figure 2f gives the current sheet thickness, determined using a fit to two-spacecraft data using a Harris current sheet model. Figure 2g gives the H^+ (black) and O^+ (blue) average pressure, and Figure 2h gives the pressure ratio. Figure 2i gives the H^+ (black) and O^+ (blue) density, and Figure 2j gives the density ratio. The substorm onset is marked by a vertical line. In these two cases, the onset was determined from dispersionless injections at geosynchronous orbit, as IMAGE FUV had no data. The similarities between the two events are striking. Both clearly show an increase in total pressure prior to substorm onset, followed by a decrease just after substorm onset, indicative of the classic loading and unloading of the magnetosphere. Both show tailward flows which begin at substorm onset, followed by earthward flows, indicating that the reconnection line first formed earthward of the spacecraft, and then moved tailward. The tailward flows are more pronounced in the nonstorm case, possibly because the satellite was located closer to the neutral sheet. Both show current sheet half-thicknesses which thin down to around 1000 km following substorm onset. There are also differences between the two events. First, the total pressure of about 1.0 nPa observed during the storm time event is significantly higher than the pressure of about 0.3 nPa observed during the nonstorm event. In addition, the pressure drops more quickly in the storm time event. Second, there is significantly more O^+ during the storm time event. This is clear in the energy spectra and both the pressure and density plots. During the storm time event, a low-energy component is present in the O^+ that is not there during nonstorm times. The O^+ density and pressure increase throughout the growth phase, but the H^+ increases as well, so that overall, the O^+/H^+ density and pressure ratios are relatively flat throughout the growth phase.
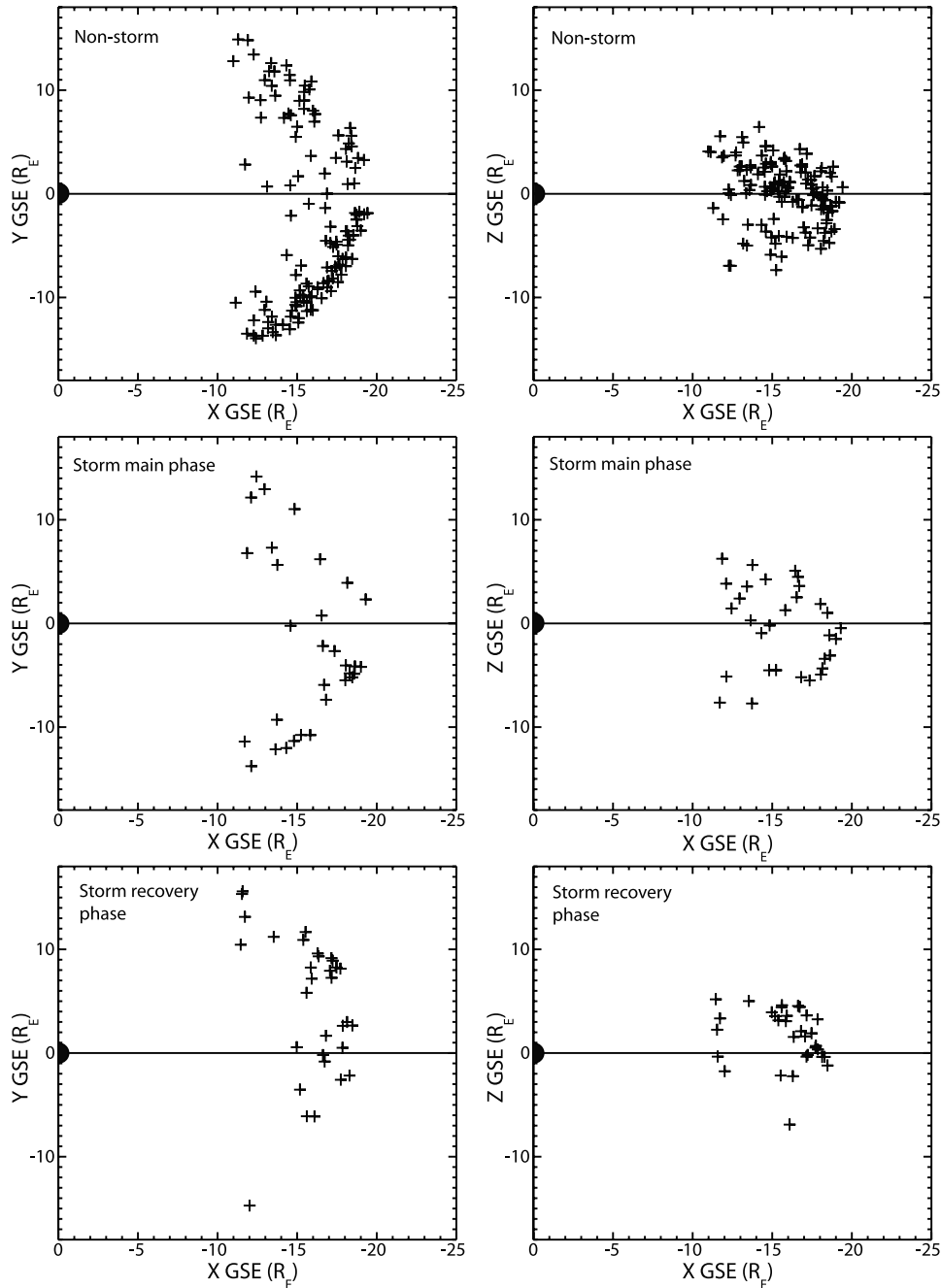
Figure 1. CLUSTER spacecraft location projected into the X-Y and X-Z GSE plane at substorm onset for the events used in this study. The events shown are only the events in which CLUSTER had data in the central plasma sheet (Beta >1). From top to bottom are the nonstorm events, the storm main phase events, and the storm recovery phase events.

[11] At substorm onset, the storm time data show a much sharper change in the energy spectra (Figures 2c and 2d) than in the nonstorm case. The H^+ becomes significantly depleted so that it is almost absent from 0942 to 0956. The O^+ is depleted below about 5 keV, but an energetic component remains. In the nonstorm case, the strong depletion is not observed, and there are only minor changes between the preonset and postonset plasma sheet spectra. These same differences are evident in the pressure and densities. In the storm time case, the H^+ density and pressure decrease much more than the O^+ just after sub-

storm onset, with the result that the O^+/H^+ ratios (Figures 2h and 2j) are the highest about 20 min after substorm onset. In the nonstorm case, the O^+/H^+ ratio remains relatively constant throughout the event, except for a few small excursions. This paper will examine whether these differences are representative of the differences between the two types of substorms.

3.2. Statistical Event Analysis
[12] The two events shown both occurred when the CLUSTER satellites were close to a neutral line. If the
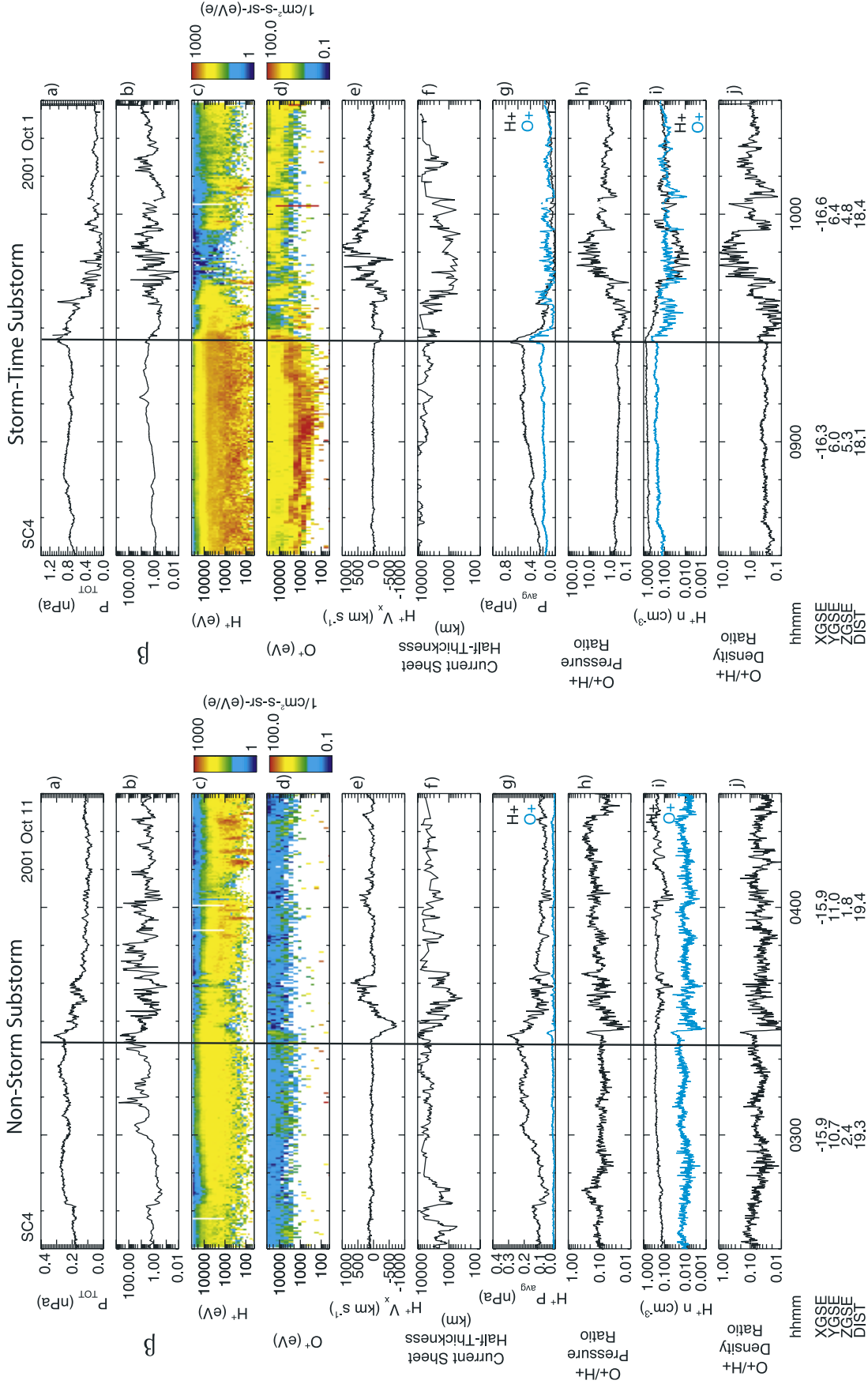
Figure 2. Data from Cluster S/C 4 for two substorms, a nonstorm substorm on 11 October 2001 from 0230 to 0430 and a storm time substorm on 11 October 2001 from 0830 to 1030. (a) The total pressure (plasma plus magnetic field), (b) the plasma beta, (c) H^+ differential flux versus energy and time, (d) O^+ differential flux versus energy and time, (e) H^+ velocity in X_{gse}, (f) the current sheet thickness, (g) H^+ (black) and O^+ (blue) pressure, (h) O^+/H^+ pressure ratio, (i) H^+ (black) and O^+ (blue) density, (j) O^+/H^+ density ratio. In both cases, substorm onset is shown with horizontal line.

Table 1. Statistical Data on When Lobe Encounters Occur During Storm Time, Storm Recovery Phase, and Nonstorm Substorms

	No Lobe	Before Onset	During Onset	At Onset	After Onset	Unclear	Total
Storm Count	4	1	8	21	10	6	50
Percent of total	8.00%	2.00%	16.00%	42.00%	20.00%	12.00%	
Percent, excluding no-lobe		2.50%	20.00%	52.50%	25.00%		
Statistical absolute error		2.53%	7.75%	14.15%	8.84%		
Recovery count	10	5	11	16	5	3	50
Percent of total	20.00%	10.00%	22.00%	32.00%	10.00%	6.00%	
Percent, excluding no-lobe		13.51%	29.73%	43.24%	13.51%		
Statistical absolute error		6.44%	10.21%	12.94%	6.44%		
Nonstorm count	73	18	42	71	18	22	244
Percent of total	29.92%	7.38%	17.21%	29.10%	7.38%	9.02%	
Percent, excluding no-lobe		12.08%	28.19%	47.65%	12.08%		
Statistical absolute error		3.01%	4.92%	6.87%	3.01%		

neutral line formed further tailward, we would not expect to see the tailward flows or such thin current sheets. *Nagai et al.* [2005] studied the location of the reconnection line during different phases of the solar cycle using Geotail. While the early Geotail results from solar minimum showed that the reconnection events were only observed outside X = −21 Re, with the highest occurrence outside 25 Re, the solar maximum results, which include the 2001–2003 period, showed the neutral line occurring between 17 and 31 Re, with approximately equal occurrence throughout this range. Thus the CLUSTER apogee is inside the average location, but well within the range where the neutral line occurs. *Nagai et al.* [2005] also found that that the location depended on solar wind input, particularly on the energy input given by $-V_x \times B_s$, where V_x is the x component of the solar wind velocity and B_s is the southward component of the interplanetary magnetic field. Thus there may be a systematic difference in where the neutral line occurs between our storm time and nonstorm time events. A systematic difference would result in different characteristics in the superposed epoch analysis due to that effect alone. In order to determine if the location of the neutral line is systematically different between our storm time and nonstorm time events, we cataloged the timing of lobe encounters for our different types of substorms. While observations of tailward flows are a strong indication that a neutral line formed earthward of the spacecraft, to make the observation requires that the spacecraft be located in the central plasma sheet at just the right time. Observations of lobe encounters are a more statistical way of determining where the spacecraft is with respect to the neutral line. If the spacecraft is sufficiently earthward of the neutral line, the plasma sheet thins during the growth phase and expands at substorm onset, due to the field dipolarization. This is the behavior typically observed at geosynchronous orbit. Thus statistically, the spacecraft would be more likely to be in the lobe before onset than after. In the vicinity of the neutral line, the plasma sheet becomes the thinnest at substorm onset, when the neutral line forms. Thus the spacecraft would be most likely to enter the lobe at onset. Each substorm was categorized according to when it entered the lobe. The categories were (1) no lobe encounter, (2) satellite entered the lobe and reentered the plasma sheet before substorm onset, (3) spacecraft entered the lobe before substorm onset and reentered the plasma sheet after substorm onset, (4) spacecraft enters lobe at onset, (5) spacecraft enters lobe after substorm onset, (6) unclear. Category 6

includes events that had multiple lobe encounters or that were in the lobe for most of the time interval so that the behavior of the plasma sheet could not be determined. Table 1 summarizes the data for the lobe encounters. For the storm time, recovery, and nonstorm substorms, Table 1 shows the number of events in each category, the percent of the total events, the percent of the events, excluding events with no lobe encounter and unclear events, and the statistical error in the percent, excluding no-lobe and unclear events. The reason for excluding no-lobe and unclear events is that they give no indication of the plasma sheet thinning and expanding behavior. The three types of events give about the same distribution of lobe encounters. In particular, the fraction of the events with a lobe encounter in which the spacecraft goes into the lobe right at onset, which is a good indication of being close to the neutral line, is 52%, 43%, and 48% for storm time, storm recovery, and nonstorm, respectively. These are the same, within the statistical error. Thus we conclude that the large-scale behavior of the plasma sheet does not vary significantly for our three types of events, and we infer from this that the average radial location of the neutral line does not vary significantly from storm time to nonstorm time in our data set. We recognize that this method is not definitive but still gives a reasonable indication, given the limited data set.

3.3. Superposed Epoch Analysis

[13] A superposed epoch analysis was performed using moments data from the CLUSTER CIS instrument and the magnetic field data from the FGM instrument. The full data set consists of H^+ and O^+ moments from the 2001–2004 time periods. We include data when the CLUSTER satellite apogee is in the magnetotail, defined to be when the satellite MLT is between 2030 and 0330. The time periods used each year cover approximately July through the middle of November. The moments are calculated from three-dimensional distributions, averaged to 1-min time resolution. S/C 4 data were mainly used because the CLUSTER/CIS instrument on S/C 4 had the best coverage for the time period. If S/C 4 data were not available, S/C 1 data were used. For each 1-min data point, a beta criterion was used to determine if the satellite was in the central plasma sheet (beta >1), the outer plasma sheet (0.1 < beta <1), or in the lobe (beta <0.1). The data were then organized by substorm onset time. The 4-hour time period around substorm onset was divided into 10-min intervals for accumulation. For each 1-min data point, the time interval and whether the satellite was in the inner plasma sheet, the outer
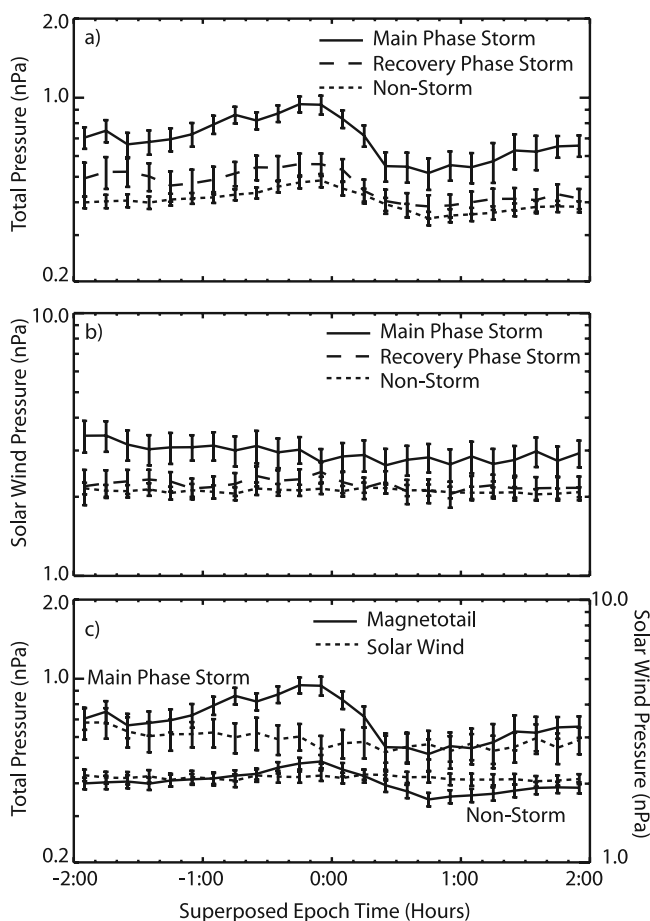
Figure 3. (a) Median total pressure in the magnetotail as a function of substorm superposed epoch time for main phase storm time (solid), recovery phase storm time (long dashed) and nonstorm (short dashed) substorms, (b) median solar wind pressures for the same substorm types, (c) overplot of total pressure (solid line) and solar wind pressure (dashed line) for the main phase storm substorms and nonstorm substorms.

plasma sheet, or the lobe was determined. The data were then added to the appropriate bin. The data points from each event in a 10-min interval were averaged. Finally, we take the median of the event averages in each time interval. The median was used to give the most representative values for each parameter. Because storm times, by definition, include the most active time periods, some very large events were found to disproportionately affect the average, while the median was not significantly affected by a few outliers.

[14] The study was done in two phases. The 2001–2002 events were first analyzed, and then an additional 2 years were added in order to obtain better statistics for the storm data. However, the solar cycle was changing during these years. The first 2 years occurred during solar maximum, while 2003 and 2004 occurred during the declining phase, and there are some systematic differences between the years. We will mainly present data from the full time period 2001–2004 analysis. We will then discuss some systematic differences that were observed as a function of time.

[15] Figure 3a shows the median total pressure (plasma pressure plus magnetic pressure) for the three substorm

types, main phase storm (solid), recovery phase storm (long-dashed), and nonstorm (short-dashed) for the 2001–2004 data set. Because there is pressure balance across the plasma sheet, we use the data from all regions (inner plasma sheet, outer plasma sheet, and lobe) to contribute to this plot. All substorm types show the standard pattern expected due to loading: the pressure increases during the growth phase of the substorm and then decreases, starting at substorm onset. The clear difference between the three lines is that the total pressure is significantly higher during the main phase storm. Figure 3b shows the median solar wind pressure during these same events. This pressure was determined using the ACE solar wind data, or WIND data if ACE was not available. The solar wind data was time-shifted to the time when it would reach the CLUSTER tail location, based on the solar wind velocity. The average solar wind pressure during the main phase storms is significantly higher than during nonstorm or recovery times, and this is then reflected in the tail pressure. In order to more easily compare the changes in the pressure, we plot the total pressure (solid line) and the solar wind pressure (dashed line) on the same plot in Figure 3c for the nonstorm and main phase storm cases. Note that the scales cover the same dynamic range, one order of magnitude, but are shifted by a factor of 5. The overall higher pressure during the main phase periods is a result of the increased solar wind pressure. However, in addition, the storm time pressure shows a greater increase during the growth phase and a faster decrease after substorm onset. The pressure during main phase reaches a minimum about 30 min after substorm onset, while the nonstorm case takes almost an hour. Thus the storm time substorms seem "bigger," with more loading and unloading. Figure 4 shows the elevation angle of the magnetic field in the central plasma sheet for the three types of substorms. The storm time substorms show a faster rise in elevation and reach a higher elevation (40 degrees) than the nonstorm substorms. This is consistent with a bigger, faster unloading during storm times.
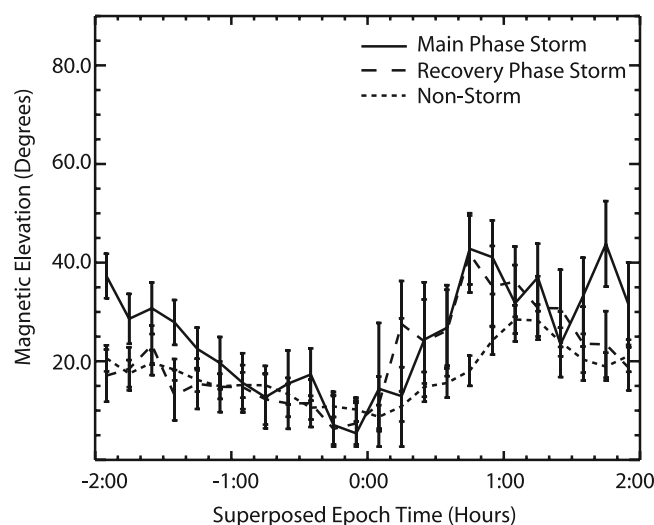

Figure 4. (a) Median magnetic elevation angle in the central plasma sheet as a function of substorm superposed epoch time for main phase storm time (solid), recovery phase storm time (long dashed), and nonstorm (short dashed) substorms.
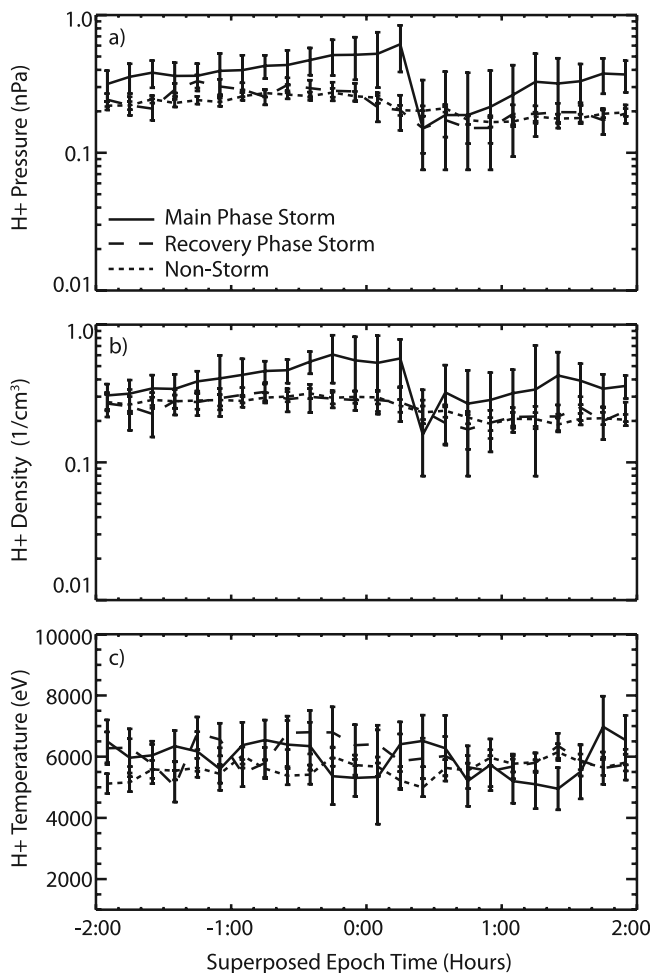
Figure 5. Median H^+ (a) pressure, (b) density, and (c) temperature in the central plasma sheet as a function of superposed epoch time for main phase storm time (solid), recovery phase storm time (long dashed), and nonstorm (short dashed) substorms.

[16] Figure 5 shows the median central plasma sheet H^+ pressure, density, and temperature. Since the pressure is carried by the plasma in the central plasma sheet, we would expect the plasma pressure to also be higher during the storm times and that is what is observed. The density profiles are very similar to the pressure profiles. The H^+ temperature is remarkably constant throughout the time period and shows little variation between events and for the different types of substorms. Note that the H^+ temperature is plotted on a linear scale so that small variations would be seen. Figure 6 shows the median central plasma sheet O^+ pressure, density, and temperature during the substorms. Again, the pressure and density show very similar profiles. The O^+ density and pressure is about a factor of 5 higher during the storm than during the nonstorm time periods. The O^+ pressure decreases more slowly after onset than the H^+ pressure. This is consistent with what was observed in our individual events. Note that after onset, when the O^+ spectra are harder, some fraction of the O^+ pressure may be missed, so the increase at substorm onset

may be greater than shown. The temperature of the O^+ shows a clear increase during the storm time substorms, and again, this may be an underestimate since there is more energetic O^+ after onset. The O^+ temperature does not change significantly for the nonstorm case.

[17] Figure 7 shows the O^+/H^+ pressure and density ratios. Overall, the O^+/H^+ ratio is highest for main phase storms and lowest for nonstorm time periods. Even for the storm time periods, the ratio remains almost constant during the growth phase. However, the pressure ratio does increase at onset for the main phase substorms. This is because there is a sudden loss of H^+ at substorm onset, while the O^+ pressure decreases more slowly, leading to the highest O^+/H^+ ratio just after onset for storm time substorms. Again, including the additional pressure from high-energy O^+ which falls outside the range of the instrument, would lead to an even greater increase of the O^+/H^+ pressure ratio at substorm onset.

[18] The data shown so far has been for the years 2001–2004. Four years are necessary to obtain statistically valid results for the storm time periods. However, there are many
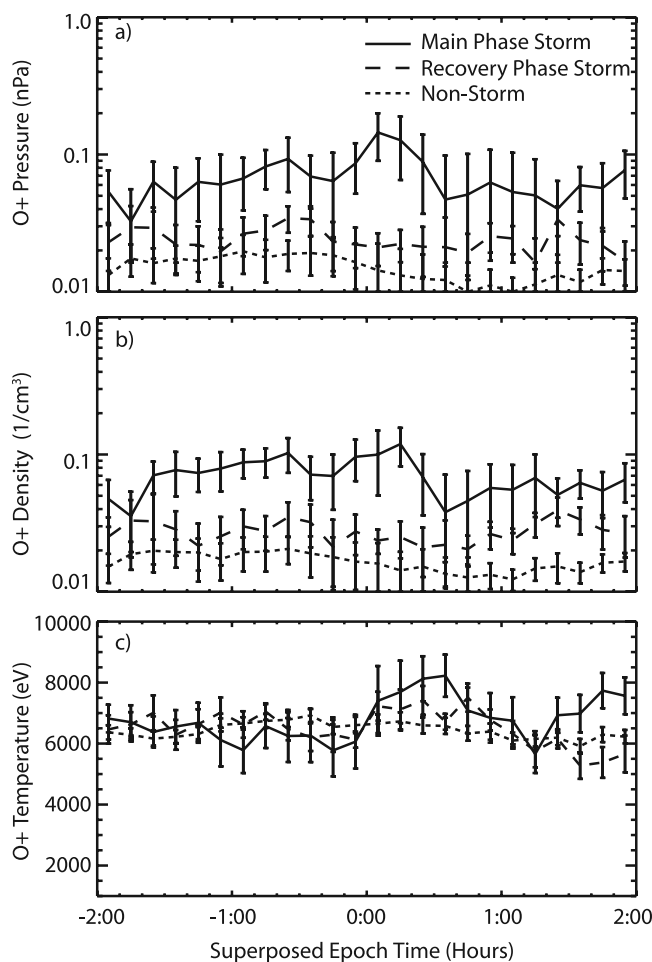

Figure 6. Median O^+ (a) pressure, (b) density, and (c) temperature in the central plasma sheet as a function of superposed epoch time for main phase storm time (solid), recovery phase storm time (long dashed), and nonstorm (short dashed) substorms.
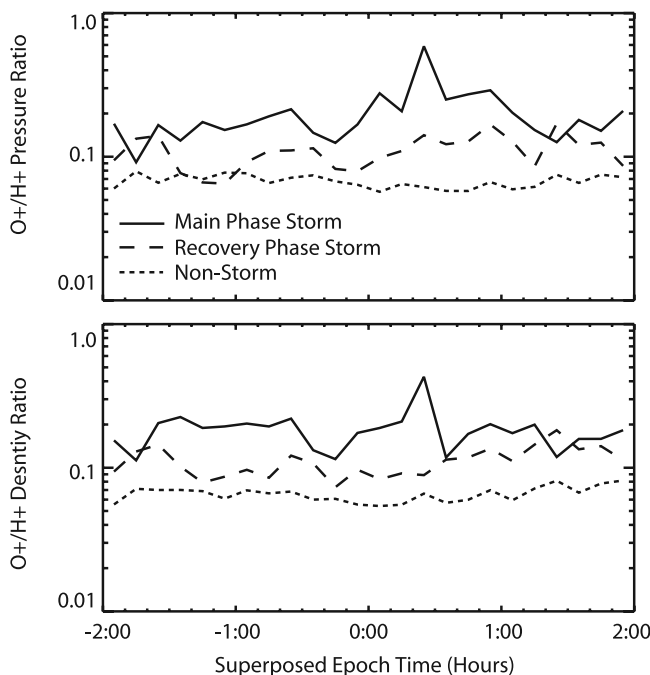
Figure 7. The O^+/H^+ (a) pressure ratio and (b) density ratio as a function of superposed epoch time for main phase storm time (solid), recovery phase storm time (long dashed), and nonstorm (short dashed) substorms.

more nonstorm substorms, so the nonstorm data can be used to look for solar cycle dependencies by comparing the solar maximum 2001–2002 data with the 2003–2004 data from the declining phase of the solar cycle. Figure 8 compares the total pressure (plasma plus magnetic field), and the central plasma sheet H^+ pressure, density, and temperature for the nonstorm substorms in the 2001–2002 time period and the 2003–2004 time period. The total pressure is lower during 2001–2002 than during 2003–2004. The average H^+ pressure in the central plasma sheet is essentially identical for the two time periods. However, the 2001–2002 time period had higher average density and lower average temperature than the 2003–2004 time period. Also, the 2001–2002 time period does show a temperature increase at substorm onset, while the 2003–2004 data shows a slight decrease. Thus the 4-year data set, shown in Figure 5c, showed no change at all. Figure 9 shows the average solar wind pressure, density, temperature, and velocity for these same nonstorm substorm time periods. With the change in the solar cycle, these parameters have changed significantly. The pressure is lower during 2001–2002 than during 2003–2004. This lower pressure is consistent with the lower pressure observed in the tail. The solar wind density is higher during 2001–2002, again consistent with observations in the plasma sheet. Finally, the solar wind velocity and temperature are both lower during 2001–2002, when the lower temperature was observed in the plasma sheet. Thus the changes in the solar wind with solar cycle change the average parameters observed in the plasma sheet during nonstorm times. The O^+ parameters for these nonstorm
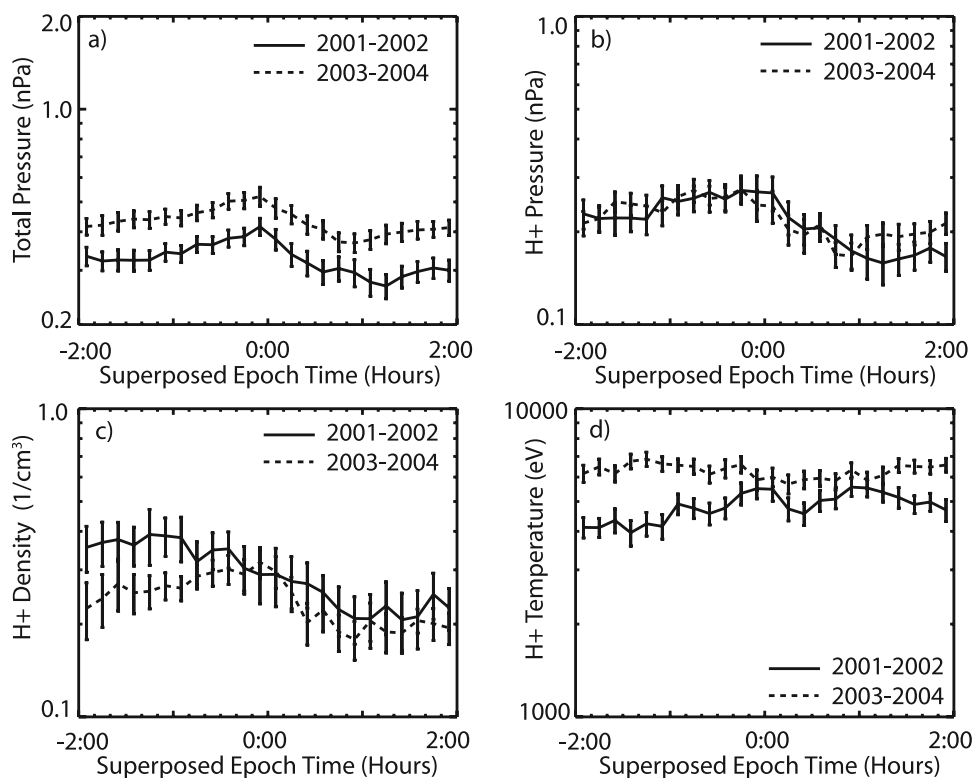

Figure 8. Comparison of (a) total magnetotail pressure and (b) central plasma sheet H^+ pressure, (c) H^+ density and (d) H^+ temperatures for the 2001–2002 and 2003–2004 nonstorm time periods.
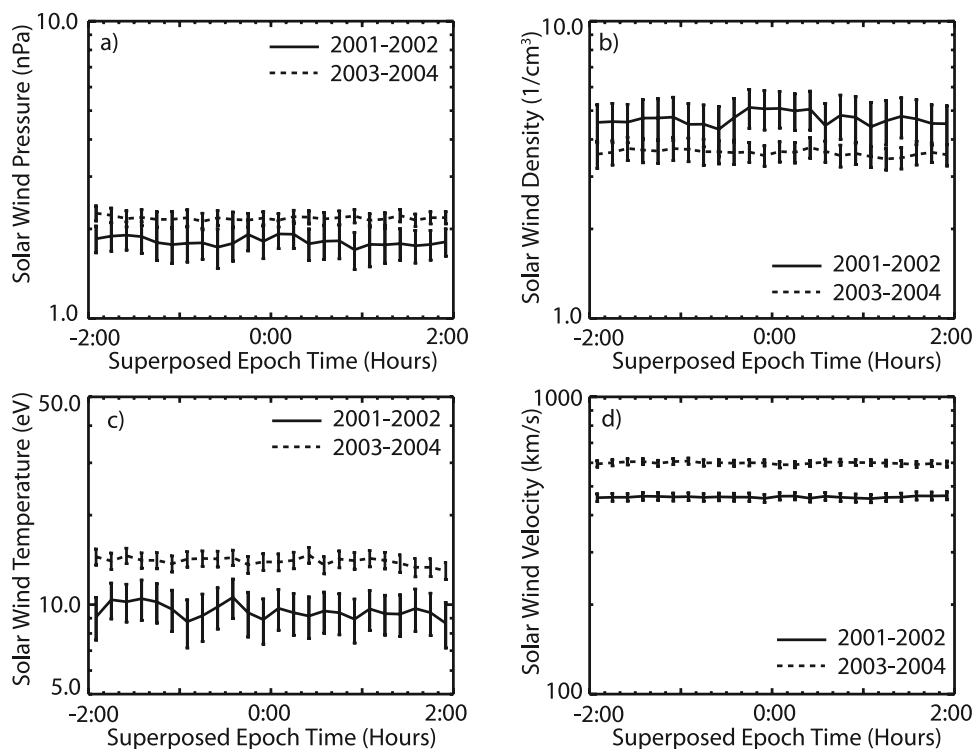
Figure 9. Comparison of (a) solar wind dynamic pressure and (b) solar wind density, (c) solar wind temperature and (d) solar wind velocity for the 2001–2002 and 2003–2004 nonstorm time periods.

substorms (not shown) were not statistically different for the nonstorm time periods in 2001–2002 and 2003–2004.

4. Discussion and Conclusions

[19] We have used 4 years of CLUSTER tail pass data to determine the statistical differences between storm time and nonstorm time substorms. The two clear differences observed between these two types of substorms are that the average O^+ content of the plasma sheet is a factor of 5 higher during storm times than during nonstorm times and that the average solar wind pressure, and therefore the average tail pressure, is a factor of 2 higher. The O^+ during storms is higher than the nonstorm cases well before substorm onset, and although the density and pressure of both H^+ and O^+ increase during the growth phase, the O^+/H^+ ratio remains relatively constant.

[20] These results are consistent with observations of outflow in the auroral regions. *Wilson et al.* [2004] used FAST/TEAMs data to determine ion outflow as a function of substorm phase. They divided substorms by apparent size and duration into small, medium, and large substorms. They found that while there was an increase in outflow at substorm onset, the bigger difference in outflow was observed between the different types of substorms. That is, the bigger substorms had more outflow during the growth phase than the smaller substorms had at their peak. During very active times, there is just more outflow overall. Similarly, in the 19 Re plasma sheet we observe that there is more O^+ overall during the very active (storm) times. If there are any additional effects of direct substorm-related outflow either during the growth phase or at onset, they are masked by the

effects of the global substorm changes, both the loading/ unloading and the changes in field-line mapping, observed in this region.

[21] H^+ and O^+ behavior during the storm time substorms differ at substorm onset. The H^+ number density and pressure both decrease more rapidly than the O^+. It is mainly the decrease in H^+ that leads to the high O^+/H^+ ratio just after onset. In addition, the O^+ temperature increases, while the H^+ temperature remains about the same. These results indicate that the effect of reconnection and magnetic field reconfiguration at onset on the H^+ and O^+ is quite different. It may be that both the H^+ and O^+ from the preonset plasma sheet are transported away from the reconnection line at onset, leaving a depleted plasma sheet but that the O^+ is then replenished more quickly. O^+ beams are observed on lobe field lines during active times [*Sauvaud et al.*, 2004] and so may enter and be heated in the reconnection process to replenish the plasma sheet. Because there is not as much H^+ on the lobe field lines, there is little direct entry of H^+ at the near-Earth reconnection site and so it is replenished more slowly. Alternatively, it may be that because of its larger gyroradius, the energetic O^+ is demagnetized so that it is not swept down the tail or earthward, along with the H^+ and low-energy O^+, when the tail reconfigures. This energetic O^+ also gets energized nonadiabatically by the crosstail electric field [*Kistler et al.*, 2005]. This could explain why the low-energy O^+ decreases at substorm onset, as observed in the storm time case in Figure 2, while the energetic O^+ increases.

[22] One puzzling result is that in contrast to the superposed epoch results of *Baumjohann et al.* [1996] and the statistical results of *Schoedel et al.* [2002], no heating of the

H^+ is observed in any of the substorms, and the H^+ temperature is not higher during storm times. Figure 8d shows that for the 2001–2002 time period, there was a modest increase in temperature, from 4 keV to 5.5 keV. The increase observed by *Baumjohann et al.* [1996] was from 2.6 to 4.3 keV for nonstorm cases and 6 to 7.7 keV for storm time cases. In both cases, the increase is about 1.7 keV, essentially the same as what we observe. Why this is only observed in the 2001–2002 case is not known. The AMPTE/IRM measurements used by Baumjohann were from solar minimum so if there were a solar cycle effect we would have expected closer agreement with the 2003–2004 time period. The most likely explanation is that the temperatures increase, if any, is small, and the differences between the years and the data sets are within the statistical variations expected from studies of this type.

[23] The comparisons of the two 2-year time periods show that the solar wind parameters affect the average plasma sheet densities and temperatures. This is consistent with *Borovsky et al.* [1998], who showed that the density of the plasma sheet is well correlated with the solar wind density, that the plasma sheet temperature is well correlated with the solar wind velocity, and that the tail pressure is correlated with the solar wind ram pressure. In addition it supports the results of *Kistler et al.* [1993], who showed that the historical measurements of tail pressure at 20 Re were well correlated with yearly averages of the solar wind dynamic pressure. The solar cycle differences in the average plasma sheet density and temperature had no effect on the substorm loading and unloading, which was identical for the two time periods.

[24] The H^+ and O^+ behavior at CLUSTER apogee of 19 Re can be contrasted with the near-Earth plasma sheet (8–9 Re) behavior. *Daglis et al.* [1990] reported an increase in O^+ energy density (pressure) during the substorm growth phase, which is greater than the H^+ increase. We also observe an increase in O^+ pressure during the growth phase in storm time substorms, but it is about the same as the H^+ so that the O^+/H^+ ratio remains about the same. Thus we do not see strong evidence for a substorm-related direct inflow of ionospheric ions during the growth phase at this radial distance. During storm times, we do observe an enhanced ionospheric input, and in particular, Figure 2b showed a low-energy component in the O^+ that is not there during nonstorm times, but this input does not increase during the growth phase. In the preonset time periods, the peak contribution to the pressure is well within the CODIF energy range, so this result is not just due to the limited energy range. The observed changes are consistent with the tail responding to the increased pressure due to the loading. If there is systematic increase in the amount of O^+ coming into the tail prior to substorm onset, it is not observed at 19 Re and therefore is not affecting reconnection onset.

[25] *Daglis and Axford* [1996] and *Nose et al.* [2005] both report observing an increase in O^+ and H^+ energy density (which is equivalent to particle pressure) at substorm onset, with a larger increase in O^+ than in H^+. At 19 Re, H^+ and O^+ densities and pressures decrease at substorm onset, with the H^+ decreasing more so that the O^+/H^+ ratio peaks just after substorm onset. This is not to say that we do not see an average energy increase at 19 Re. In our energy range, we do observe that the O^+ energy is higher after substorm

onset, as shown in Figure 2. *Moebius et al.* [1987], using the SULEICA instrument on AMPTE/IRM clearly showed the flux increases of the energetic (>40 keV) ions at substorm onset in this same 19 Re region, and *Kistler et al.* [1990] showed that the spectral changes were very similar at IRM apogee of 18.8 Re and CCE apogee of 8.8 Re. The different energy ranges covered by the two studies explain part of the difference. *Nose et al.* [2005] includes energies from 9 to 210 keV/e and *Daglis and Axford* [1996] includes energies from 1 to 300 keV/e, while the moments in this paper include 40 eV to 40 keV. Thus the energy range for this study contains a better density measurement but is missing some pressure, particularly for O^+. However, the main difference between the two regions can be understood from the differences in the plasma sheet dynamics at the two locations. The pressure in the tail-like plasma sheet at 19 Re is dominated by the solar wind, and so the pressure increases and decreases are controlled by the loading/unloading behavior. Since the particles carry the majority of the pressure in the central plasma sheet, these same pressure changes are observed in the particle pressure. At 8–9 Re, the field shows the stretching and dipolarization but not the increases and decreases in the total pressure. In fact, the total pressure generally increases at substorm onset in the near-Earth plasma sheet region, when the field dipolarizes [*Kistler et al.*, 1992]. In addition, in the stronger magnetic field at 8–9 Re, the particles are not carrying the majority of the pressure, so their pressure does not necessarily reflect the changing external conditions. At 19 Re, the ions are accelerated and heated, as they are further in, but because pressure balance must be maintained in the tail, the total energy density is still observed to decrease at substorm onset.

[26] The high O^+ content and high pressure observed during storm time substorms lead to different initial conditions for reconnection, and it is intriguing to consider whether these differences cause the differences in the substorms. The main difference between storm and nonstorm substorms is that the pressure increase (i.e., the loading) is greater during a storm time substorm and the pressure decrease is faster. In addition, the magnetic field elevation change is greater and faster after substorm onset during storm time substorms, consistent with the results of *Baumjohann et al.* [1996] but in contrast to the results of *McPherron and Hsu* [2002]. If the reason for the difference in the substorms is the enhanced O^+, the results are in contrast with the expected effects of heavy ions on reconnection. If the fast unloading indicates a fast reconnection rate, that is opposite to the expectation based on the decreased Alfven speed. Similarly, if the O^+ decreases the threshold for reconnection onset, we would expect the onset to occur after less loading of the magnetosphere. Instead, more loading is observed. There have been many different trigger mechanisms suggested for substorm onset, some involving internal instabilities and some involving external triggering. That O^+ does not have the expected effect of decreasing the threshold for reconnection onset indicates that a triggering mechanism other than the ion tearing mode instability at the reconnection site is responsible for onset. Unraveling the role that O^+ does play will require more detailed studies of the microphysics in this region.

References

Baker, D. N., E. W. Hones Jr., D. T. Young, and J. Birn (1982), The possible role of ionospheric oxygen in the initiation and development of plasma sheet instabilities, *Geophys. Res. Lett*, 9, 1337.

Baker, D. N., T. A. Fritz, W. Lennartsson, B. Wilken, H. W. Kroehl, and J. Birn (1985), The role of heavy ions in the localization of substorm disturbances on March 22, 1979: CDAW 6, *J. Geophys. Res.*, 90, 1273.

Balogh, A., et al. (2001), The Cluster magnetic field investigation: Overview of in-flight performance and initial results, *Ann. Geophys.*, 19, 1207.

Baumjohann, W., Y. Kamide, and R. Nakamura (1996), Substorms, storms, and the near-Earth tail, *J. Geomagn. Geoelectr.*, 48, 177.

Borovsky, J. E., M. F. Thomsen, and R. C. Elphic (1998), The driving of the plasma sheet by the solar wind, *J. Geophys. Res.*, 103, 17,617.

Daglis, I. A., and W. I. Axford (1996), Fast ionospheric response to enhanced activity in geospace: Ion feeding of the inner magnetosphere, *J. Geophys. Res.*, 101, 504.

Daglis, I. A., and E. T. Sarris (1998), Comment on "Experimental investigation of possible geomagnetic feedback from energetic (0.1 to 16 keV) terrestrial O+ ions in the magnetotail current sheet", *J. Geophys. Res.*, 103, 29,545.

Daglis, I. A., E. T. Sarris, and G. Kremser (1990), Indications for ionospheric participation in the substorm process from AMPTE/CCE observations, *Geophys. Res. Lett.*, 17, 57.

Frey, H. U., S. B. Mende, V. Angelopoulos, and E. F. Donovan (2004), Substorm onset observations by IMAGE-FUV, *J. Geophys. Res.*, 109, A10304, doi:10.1029/2004JA010607.

Fu, S. Y., Q. G. Zong, T. A. Fritz, Z. Y. Pu, and B. Wilken (2002), Composition signatures in ion injections and its dependence on geomagnetic conditions, *J. Geophys. Res.*, 107(A10), 1299, doi:10.1029/2001JA002006.

Grande, M., C. H. Perry, A. Hall, J. Fennell, R. Nakamura, and Y. Kamide (2003), What is the effect of substorms on the ring current ion population during a geomagnetic storm?, in *Disturbances in Geospace: The Storm-Substorm Relationship, Geophys. Monogr. Ser.*, vol. 142, edited by A. S. Sharma, Y. Kamide, and G. S. Lakahini, p. 75, AGU, Washington, D. C.

Kistler, L. M., E. Moebius, B. Klecker, G. Gloeckler, F. M. Ipavich, and D. C. Hamilton (1990), Spatial variations in the suprathermal ion distributions during substorms in the plasma sheet, *J. Geophys. Res.*, 95, 18,871.

Kistler, L. M., E. Moebius, W. Baumjohann, G. Paschmann, and D. C. Hamilton (1992), Pressure changes in the plasma sheet during substorm injections, *J. Geophys. Res.*, 97, 2973.

Kistler, L. M., W. Baumjohann, T. Nagai, and E. Moebius (1993), Superposed epoch analysis of pressure and magnetic field configuration changes in the plasma sheet, *J. Geophys. Res.*, 98, 9249.

Kistler, L. M., et al. (2005), Contribution of nonadiabatic ions to the cross-tail current in an O+ dominated thin current sheet, *J. Geophys. Res.*, 110, A06213, doi:10.1029/2004JA010653.

Korth, A., R. H. W. Friedel, M. G. Henderson, F. Frutos-Alfaro, and C. G. Mouikis (2003), O+ transport into the ring current: storm versus substorm, in *Disturbances in Geospace: The Storm-Substorm Relationship, Geophys. Monogr. Ser.*, vol. 142, edited by A. S. Sharma, Y. Kamide, and G. S. Lakahini, p. 59, AGU, Washington, D. C.

Lennartsson, W., and E. G. Shelley (1986), Survey of 0.1- to 16 keV/e plasma sheet ion composition, *J. Geophys. Res.*, 91, 3061.

Lennartsson, O. W., D. M. Klumpar, E. G. Shelley, and J. M. Quinn (1993), Experimental investigation of possible geomagnetic feedback from energetic (0.1 to 1 keV) terrestrial O+ ions in the magnetotail current sheet, *J. Geophys. Res.*, 98, 19,443.

McPherron, R. L., and T.-S. Hsu (2002), A comparison of substorms occurring during magnetic storms with those occurring during quiet times, *J. Geophys. Res.*, 107(A9), 1259, doi:10.1029/2001JA002008.

Moebius, E., M. Scholer, B. Klecker, D. Hovestadt, G. Gloecker, and F. M. Ipavich (1987), Acceleration of ions of ionospheric origin in the plasma sheet during substorm activity, in *Magnetotail Physics*, edited by A. T. Y. Lui, pp. 231–234, Johns Hopkins Univ. Press, Baltimore, Md.

Nagai, T., M. Fujimoto, R. Nakamura, W. Baumjohann, A. Ieda, I. Shinohara, S. Machida, Y. Saito, and T. Mukai (2005), Solar wind control of the radial distance of the magnetic reconnection site in the magnetotail, *J. Geophys. Res.*, 110, A09208, doi:10.1029/2005JA011207.

Nose, M., S. Taguchi, K. Hosokawa, S. P. Christon, R. W. McEntire, T. E. Moore, and M. R. Collier (2005), Overwhelming O+ contribution to the plasma sheet energy density during the October 2003 superstorm: Geotail/EPIC and IMAGE/LENA observations, *J. Geophys. Res.*, 101, A09S24, doi:10.1029/2004JA010930.

Oieroset, M., M. Yamauchi, L. Liszka, S. P. Christon, and B. Hultqvist (1999), A statistical study of ion beams and conics from the dayside ionosphere during different phases of a substorm, *J. Geophys. Res.*, 103, 6987.

Reme, H., et al. (2001), First multispacecraft ion measurements in and near the earth's magnetosphere with the identical CLUSTER Ion Spectrometry (CIS) experiment, *Ann. Geophys.*, 19, 1303.

Sauvaud, J.-A., et al. (2004), Case studies of the dynamics of ionospheric ions in the Earth's magnetotail, *J. Geophys. Res.*, 109, A01212, doi:10.1029/2003JA009996.

Schoedel, R., K. Dierschke, W. Baumjohann, R. Nakamura, and T. Mukai (2002), The storm time central plasma sheet, *Ann, Geophys.*, 20, 1737.

Shay, M. A., and M. Swisdak (2004), Three-species collosionless reconnection: effect of O+ on magnetotail reconnection, *Phys. Rev. Lett.*, 93, 1975001.

Wilson, G. R., D. M. Ober, G. A. Germany, and E. J. Lund (2004), Nightside auroral zone and polar cap ion outflow as a function of substorm size and phase, *J. Geophys. Res.*, 109, A02206, doi:10.1029/2003JA009835.

Winglee, R. M. (2003), Circulation of ionospheric and solar wind particle populations during extended southward interplanetary magnetic field, *J. Geophys. Res.*, 108(A10), 1385, doi:10.1029/2002JA009819.

Yau, A. W., B. A. Whalen, W. K. Peterson, and E. G. Shelley (1984), Distribution of upflowing ionospheric ions in the high-altitude polar cap and auroral ionosphere, *J. Geophys. Res.*, 89, 5507.

Yau, A. W., E. G. Shelley, W. K. Peterson, and L. Lenchyshyn (1985), Energetic auroral and polar ion outflow at DE 1 altitudes: Magnitude, composition, magnetic activity dependence, and long-term variations, *J. Geophys. Res.*, 90, 8417.

―――――――――
X. Cao, L. M. Kistler, and C. G. Mouikis, Space Science Center, University of New Hampshire, Morse Hall, 39 College Road, Durham, NH 03824, USA. (lynn.kistler@unh.edu)

I. Dandouras, Centre d'Etude Spatiale des Rayonnements, 9 Avenue Colonel-Rpche, BP 4346, F-31029 Toulouse, France.

H. Frey, Space Sciences Laboratory, University of California, Berkeley, 7 Gauss Way, Berkeley, CA 94720-7450, USA.

R. Friedel, Space and Science Application, Los Alamos National Laboratory, ISR-1 MD-D466, Los Alamos, NM 87545-0000, USA.

B. Klecker, Max Planck Institut für Extraterrestriche Physik, Karl-Schwarzschild Strasse 1, Postfach 1312, D-85740 Garching bei München, Germany.

A. Korth, Max-Planck-Institut für Aeronomie, Max-Planck Strasse 2, Postfach 20, D-37191 Katlenburg-Lindau, Germany.

E. Lucek, Space and Atmospheric Physics Group, Blacket Laboratory, Imperial College London, London, SW7 2BW, UK.

R. Lundin, Swedish Institute of Space Physics, P. O. Box 812, S-981 28 Kiruna, Sweden.

M. F. Marcucci, Istituto Fisica dello Spazio Interplanetario, Via del Fosso del Cavaliere, 100, I-00133 Rome, Italy.

M. McCarthy, Geophysics Program, University of Washington, ATG Building, Box 351650, Seattle, WA 98195, USA.